Circuit Techniques for Miniaturized Biomedical Sensors

Inhee Lee[1], Yejoong Kim[1], Suyoung Bang[1], Gyouho Kim[1], Hyunsoo Ha[2], Yen-Po Chen[1], Dongsuk Jeon[1], Seokhyun Jeong[1], Wanyeong Jung[1], Mohammad Hassan Ghaed[1], Zhiyoong Foo[1], Yoonmyung Lee[1], Jae-Yoon Sim[2], Dennis Sylvester[1], and David Blaauw[1]

[1] University of Michigan, Ann Arbor, MI, USA
[2] Pohang University of Science and Technology, Pohang, Korea

***Abstract* — Miniaturized biomedical sensors promise improved quality of medical diagnosis and treatment. However, the realization of such implantable devices faces challenges due to limited battery capacity and energy sources. This paper describes new circuit techniques for miniaturized biomedical sensors, with particular emphasis on bio-signals sensing front end, power management, and communication.**

I. Introduction

Biomedical sensors enable new methods of diagnostics, drug delivery, neural prosthetics, tissue engineering, and minimally invasive surgery. As a result such sensors have become an attractive solution to meet the ever-growing demand for high-quality medical care [1], [2]. In particular, a number of small biomedical systems have been proposed that offer advantages such as better quality of care, shorter hospitalization, and reduction of pain and medical complications; these include ECG monitors [3]-[5], intraocular pressure monitors [6]-[8], and neural recorders [9]-[11]. In addition, miniature, lightweight, and implantable bio-sensing microsystems are useful for animal-based research as they minimize animal post-implant trauma and stress-induced signal distortion [12]. Today, extremely miniaturized systems are being developed that can be injected in patients through a syringe needle for health-monitoring and patient-centric healthcare [4], [13], [14].

However, realizing such a small system poses challenges due to limited battery capacity and energy sources. As shown in Fig. 1 [15], 0.1~1mW can be drawn continuously for a year from conventional alkaline AA and 20mm Li coin batteries. In contrast, only ~1nW is feasible for the same lifetime using 1mm^2 Li thin-film battery [16]. An energy harvester increases the maximum usable power and lifetime. However, 1mm^2 CMOS solar cell generates ~30nW in indoor light condition, and thus it raises the allowable power budget to only ~10nW when accounting for energy conversion/storage efficiencies. Battery replacement in implantable biomedical sensors (which must be done through surgery) is expensive and incurs risk. Hence, to achieve long lifetime or energy autonomy in the limited form factor, low-power circuit design is paramount.

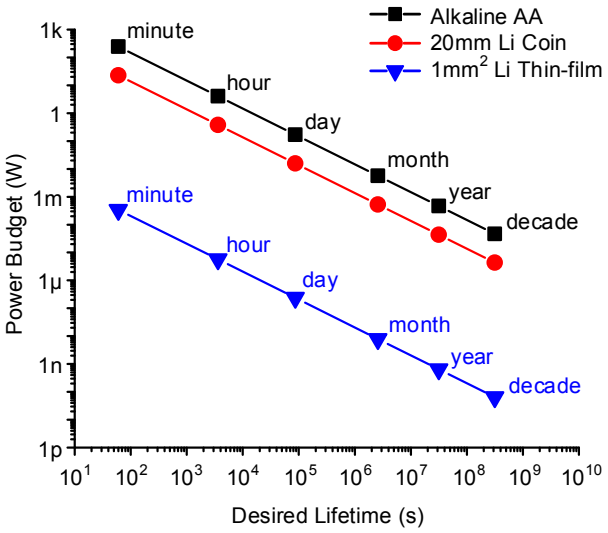

Fig. 1. Power budget for desired lifetime in different batteries.

In this paper a miniaturized biomedical sensing system is described in Section II, and low-power circuit techniques for bio-signals sensing front end, power management, and communication are discussed in Sections III, IV, and V, respectively.

II. System Overview

A mm^3-scale sensing system platform is shown in Fig. 2 with a heterogeneous stackable multi-layer structure [17]. Power delivery and inter-layer communication are performed through a wirebonding scheme, where the number of I/O signals are limited by the aggressive form factor. Additional layers can be simply inserted in this die-stacked architecture. For different applications, users can build their own biomedical sensor by selecting the necessary layers and designing an application-specific layer in a preferred technology.

978-1-4799-3286-3/14/$31.00 ©2014 IEEE

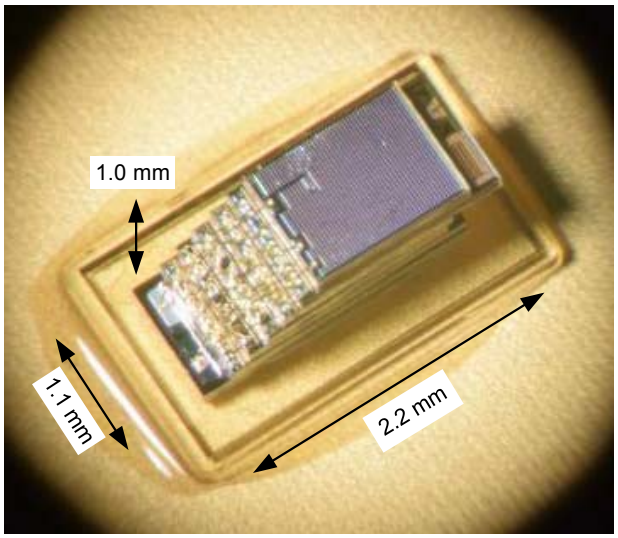

(a)

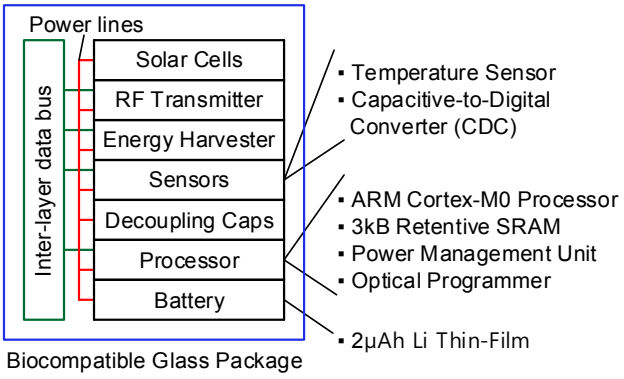

(b)

Fig. 2. Miniaturized biomedical sensing system (a) Photograph (b) System diagram.

The sensor can be encapsulated in a glass package [7]. The sealed glass container demonstrated biocompatibility through implantation and *in vivo* measurements [18]-[20]. Also, the cavity inside the glass container can be filled with dark epoxy to block light since high leakage currents are generated in low-power circuits from strong light [21]. However, parts that require light should not be shielded, e.g., harvesting and optical communication.

In the processor layer, an ARM® Cortex-M0 processor and 3kB of always-on low leakage retentive SRAM are designed in a 180nm CMOS technology process and manage the system. Other than these main control circuits, vital components include bio-signals sensing front end, power management, and communication. The next sections discuss circuits designed for these sub-systems, which are integrated in the system above.

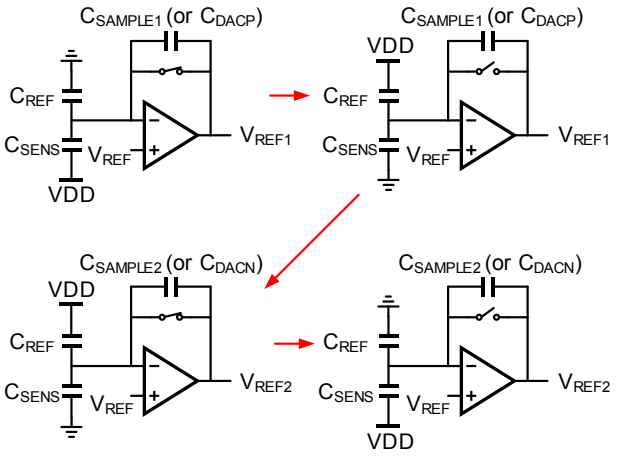

Fig. 3. Operation of front end in low-power capacitive-to-digital converter.

III. Bio-Signal Sensing Front End

A. Capacitance-to-Digital Converter (CDC)

Capacitive sensing is widely adopted (e.g., pressure [22], displacement [23], and humidity [24]) for low-power applications due to the zero static current requirement for signal readout. CDCs have been designed to achieve high resolution with low power consumption. Sigma-delta converters offer high resolution, but the energy per conversion is poor since they repeatedly charge and discharge the large sensor capacitor (e.g., 5–70pF) [23], [24]. For better energy efficiency, the sensor capacitor can be connected to a capacitor DAC (CDAC) in a SAR ADC, but this approach has the drawback of significantly reduced voltage swing at the comparator input, which limits the achievable resolution [22]. Thus, the best figure-of-merit (FOM) for a CDC is several pJ/conversion-step, which is much worse than ADCs that can achieve sub-10fJ/conversion-step [25].

However, the CDC in [26] employs the readout front end with correlated double sampling (CDS) and achieves the figure-of-merit (FOM) of 63.9fJ/conversion-step. This energy-efficient CDC is suitable to burst conversion with intermittent operation, which is common in duty-cycled low-power sensors.

The CDC has two main phases of operation: CDS and A-D conversion. Fig. 3 shows the CDS operation including a sensor capacitor (C_{SENS}), a reference capacitor (C_{REF}), a sampling capacitor (C_{SAMPLE} or C_{DAC}), and an amplifier. A key feature is that the effect of variations on V_{REF} and offset voltage (V_{OS}) are all cancelled by the CDS and differential configuration. Also, parasitic capacitance (10s of pF) due to off-chip C_{SENS} does not

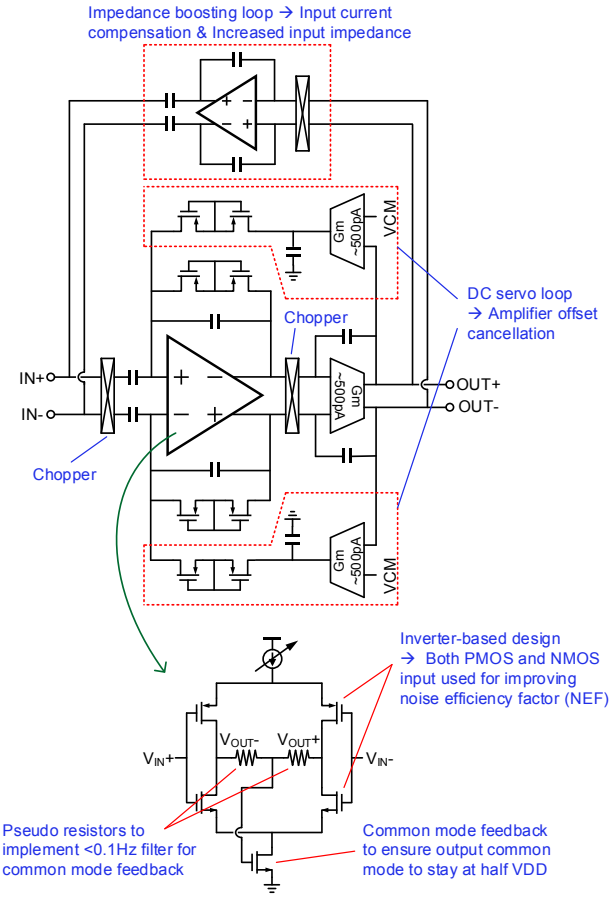

Fig. 4. First stage amplifier of analog front end in implantable ECG monitor.

cause any issues since the node between C_{REF} and C_{SENS} is held as the virtual ground by negative feedback formed by the amplifier. In A-D conversion, $C_{SAMPLE1}$ and $C_{SAMPLE2}$ become the differential CDAC in a SAR ADC. The amplifier is turned off for power reduction, and typical asynchronous SAR ADC operation begins for 13b digital output.

B. Electrocardiography (ECG) Analog Front End

ECG is a critical source of information used to identify a number of heart disorders. Due to the extremely small amplitude (~μV), the signal is susceptible to noise from 60Hz power and body movement. To avoid these issues, [4] described an implantable ECG monitor. An implanted sensor is less prone to such noise sources and also can use closer-spaced electrodes without signal degradation since it has greater proximity to the heart [27]. Moreover, it allows continuous monitoring without disturbing patient quality of life (as is common in wearable devices).

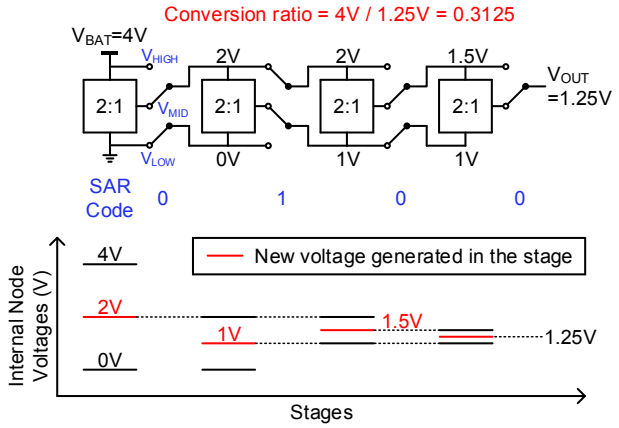

Fig. 5. An example of 4-stage successive approximate operation in capacitive step-down converter.

The challenge here is low-power operation between battery recharge events. For a syringe-implantable ECG recording and analysis device, the system width and length are limited to 1.5mm and 2cm, respectively. The length is sufficient for two electrodes to give an acceptable potential difference. In this limited form factor, 167nW system power consumption (typically 10–30μW in previous works [28]-[30]) is required when considering an on-chip 5μAh thin-film Li battery and 5-day lifetime to provide margin for expected nightly wireless battery recharging.

The AFE includes a low-noise instrumentation amplifier, a variable-gain amplifier, and a SAR ADC. The first stage of the amplifier in Fig. 4 dominates total AFE power consumption to achieve low noise. For high noise efficiency, an inverter-based amplifier is selected and is biased in the subthreshold regime with a 9μV noise floor, which allows the system to accurately detect arrhythmia. A DC servo loop helps the inverter-based design to stabilize the differential output to half supply voltage. Also, AC coupling and an impedance-boosting loop are employed for very high input impedance required due to large tissue-electrode impedance.

IV. Power Management

A. Step-Down Converter

Battery voltages (e.g., 3.2~4V for Li battery) are typically higher than the supply voltage required for analog and digital circuits (e.g., 1~2V), necessitating a DC-DC down converter. A linear regulator results in low efficiency due to high voltage conversion ratio. An inductor-based switching converter needs a bulky off-chip inductor for reasonable switching frequency, which is not

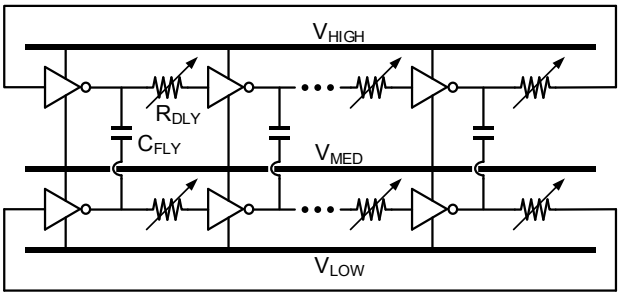

Fig. 6. Self-oscillating voltage doubler for low-power energy harvester.

acceptable in miniaturized biomedical application. Thus, a capacitive switching converter is preferred since it can utilize fully integrated, on-chip capacitors and achieve high efficiency [31]-[33]. However, the converter typically suffers from coarse output voltage resolution. Typically, the number of capacitors limits the possible number of conversion ratios.

The capacitive switching converter in [34] overcomes this limitation by using binary searching approach in order to offer a wide-range of output voltages. It provides an output voltage range of 0.4 to 4V, with 7b 31mV step resolution, achieving 72% peak efficiency. The converter consists of a 4:1 ladder switched-capacitor (SC) converter and five cascaded 2:1 SC stages. In order to obtain a fine grain output voltage, V_{HIGH} and V_{LOW} of each SC stage are connected to V_{HIGH} & V_{MID} or V_{MID} & V_{LOW} in the previous stage as shown in Fig. 5. The decision is made in successive approximate fashion by comparing the voltage to a target output voltage. The SAR SC converter can obtain the resolution of $V_{BAT}/2^{\#stage}$ while a ladder one has V_{BAT}/#stage under no load condition.

B. Energy Harvester

In a miniaturized system, energy capacity of the battery is limited due to the small form factor. Energy harvester is a solution to overcome this constraint and extend battery lifetime to perpetual operation. However, the energy source needs to be small in size, and thus the energy generated is also limited. For instance, a mm-scale solar cell offers only 10s of nW in indoor condition. A SC converter is preferred to a boost DC-DC converter since it does not require a large off-chip component [35]-[37]. However, designing an efficient DC-DC step-up converter is extremely challenging at the low power level.

The SC energy harvester in [38] improves energy efficiency by removing the overheads in clock generation and level-conversion to drive the switched capacitors. It converts 7nW input power from 250mV to 4V and maintains 35% end-to-end efficiency with < 1mm^2 solar

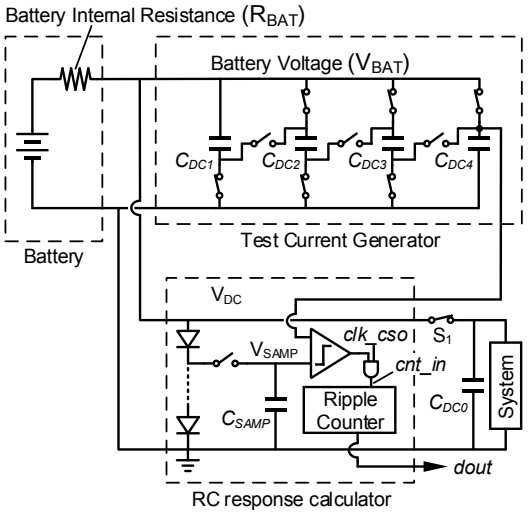

Fig. 7. Battery resistance monitor circuit to check battery health degradation.

cell in 260 Lux indoor light condition. It is enabled by a SC voltage doubler in Fig. 6 that completely internalizes an oscillator in time-interleaved structure. The voltage doubler consists of two stacked ring oscillators, and each stage is connected by flying capacitors (C_{FLY}). Inverters in the ring oscillators charge and discharge the flying capacitors and transfer charge from the lower to the upper stair. Also, the inverters drive the next stage in the ring oscillator, thereby forming a multi-phase SC converter. Its oscillation self-starts and harvests energy with > 140mV input voltage. A delay element (R_{DLY}) helps match the charging or discharging time of the flying capacitors to the oscillation period. The delay automatically balances switching and conduction losses across a 5nW to 5µW load current, which enables idle power consumption less than 3nW.

C. Battery Resistance-to-Digital Converter

Due to the limited form factor, miniaturized sensors employ very small batteries with high battery resistance (e.g. 7kΩ [15]). Over multiple charge cycles, the battery resistance increases, which indicates battery health degradation (e.g. 7 to 31kΩ over 1000 cycles [16]) [39]. Thus, the resistance information can be used to determine the state of charge (SOC) in the battery in conjunction with temperature and zero-load battery voltage [40]. The SOC allows the battery-operated system to update its power strategy and extend lifetime.

The battery resistance monitor in [41] includes a test current generator and RC response calculator as shown in Fig. 7. The test current generator first connects test capacitors in series to discharge them. If the capacitors are suddenly configured in this way, a very high voltage will

be applied to the following circuits that can damage them. Thus, they are gradually connected in series, which gives enough time for the voltage on the capacitors to be stabilized to acceptable levels. Here, 8 test capacitors are used (4 shown in Fig. 7), and overshoot on the battery voltage is limited to 5.6%. Note that the test capacitors act as standard decoupling capacitors in default operation. Next, all the stacked capacitors are connected to battery in parallel at the same time. This draws a large current from the battery and creates an RC voltage curve on the battery voltage. Since its time constant is proportional to battery resistance, the rising time of the voltage curve is measured using the RC response calculator with pre-sampled voltage (V_{SAMP}) and a supply-insensitive oscillator. During the RC current generation, the system is disconnected to be protected from the test-induced voltage drop. For this period, the system relies on the charge in the decoupling capacitor, and thus the test event takes only < 65µs. The battery resistance monitor generates 6b digital output with 10nJ/conversion, including all the control clock generation.

V. Communication

A. Optical Wake-up Receiver

In order to program/reprogram the miniaturized biomedical sensors, a receiver needs to keep monitoring signals that match to their communication protocol. This continuous operation should be implemented within low power since battery lifetime is mainly determined by standby power due to heavy duty-cycling. Wire connection is not an option due to limited size, inaccessibility after deployment [17], and higher chance of infection [3]. RF and ultrasound solutions have been used as a wake-up receiver, but their power is in the µW range and is not acceptable in the sensor system with nW level standby power [42]-[44].

A wake-up receiver using an optical approach in [45] consumes 695pW in standby mode and 140pJ/bit at 91bps in active mode. The receiver converts light intensity modulated by a transmitter to digital format. Solar cells are implemented as n+/pw/nw parasitic diodes, and generate an open circuit voltage of ~ 250mV. This voltage changes logarithmically by illumination. A comparator gives a bit of 1 if solar cell output voltage is higher than the 190mV reference voltage. One key challenge in this optical approach is to distinguish high and low light intensity from the optical transmitter in the presence of ambient light. In order to dramatically change solar cell output voltage between the different illuminations, a tunable pull-down resistance is added to a solar cell in

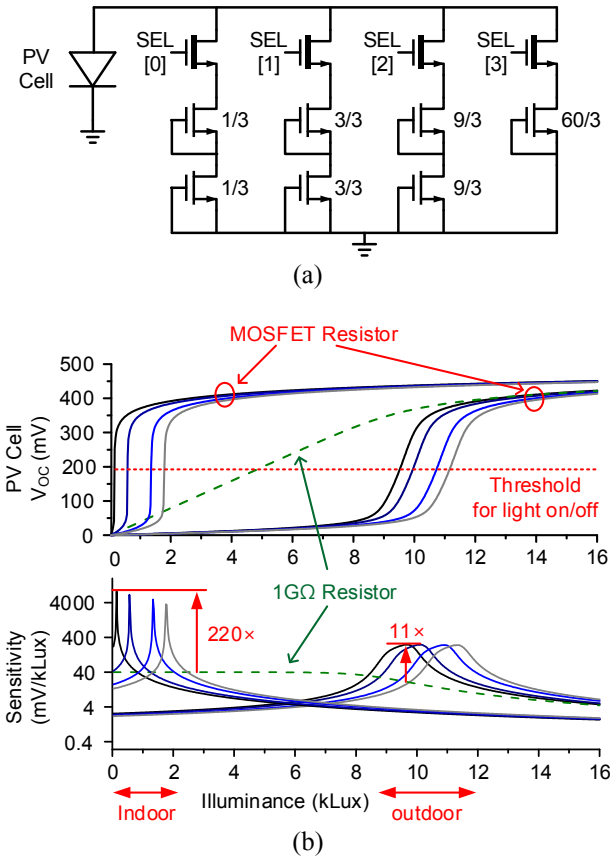

Fig. 8. Front end for a low-power optical wake-up receiver (a) PV cell with non-linear resistance (b) Increased sensitivity by non-linear resistor.

parallel as shown in Fig. 8 (a). However, an on-chip linear resistor is not a practical option since 100s of MΩ is required to modulate the small solar cell current and this takes a prohibitively large die area. Instead of a linear resistor, non-linear off-state MOSFET resistance is employed. The non-linear resistance changes abruptly from low to high as illumination increases since subthreshold current has exponential dependence on V_{DS}. This design improves the sensitivity to light detection by 220× and 11× in indoor and outdoor condition, respectively, compared to a 1GΩ linear resistor as shown in Fig. 8(b). The optical front ends, each including a photodiode and a pull-down resistor, are placed in three different locations, and their outputs are majority-voted so as to improve robustness against false trigger. Slightly sacrificing standby power, this redundancy offers immunity against possible structural problems (e.g. a dust particle blocking the diode).

B. Radio Transmission

RF transmission techniques can be used for implantable sensors, but the usage is limited by antenna size and

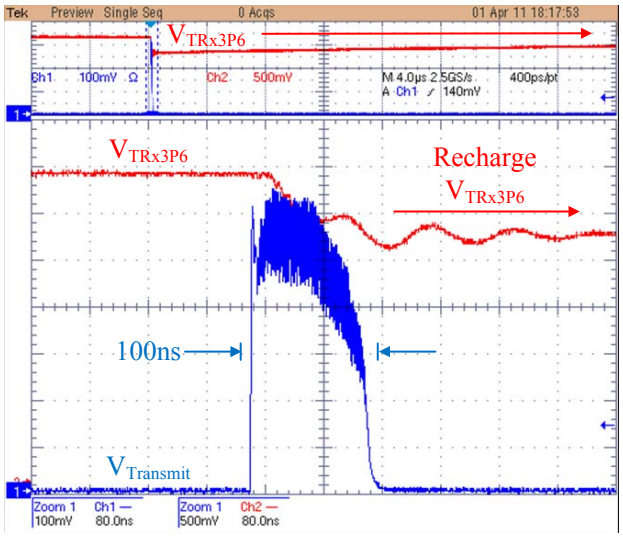

Fig. 9. Local supply voltage supported by decoupling capacitance during radio transmission.

power budget constraints. Passive backscattering solutions modulate impedance and reflect an incoming RF signal. It moves power consumption to a modulator, which is the separate device and has less power limitation on the sensor node itself. However, in spite of low power consumption, 3.5~4.0 cm antenna is necessary for ~10^{-6} BER over 1.5~2.0 cm transmission channel [46], [47], which makes it unacceptable for miniaturized sensor nodes. Also, the large antenna makes the implanted sensors incompatible with MRI machines [3]. Active techniques obtain better transmit performance using smaller antenna or coils (e.g. 20.4nJ/bit with 0.47 mm coils [6], [48]-[50]). However, a small battery cannot support the ~mA peak current required for an RF transmitter.

Radio transmission implemented in [7] utilizes a local charge reservoir to avoid the low instantaneous current limitation in millimeter scale batteries. To realize the small form factor, high-capacity off-chip capacitor cannot be used. Thus, a 1.6nF of MOS and MIM capacitors are integrated as local charge storage on-chip. The capacitance is the maximum value that does not violate the system area constraint of 1.8mm^2. Considering the decoupling capacitance, data transmission speed should be carefully decided so as not to damage the battery and system operation. For a single 100ns pulse at a time, the power consumption of transmitter drops the local capacitor voltage by < 25% as shown in Fig. 9. The voltage is recovered in the next 131µs through the battery, drawing an 11µA current. The recharging speed is limited by a resistor to protect battery from a high charging current. The effective data rate is 7.5kb/sec, and the system can transmit daily IOP data measured every 15 minutes in 130ms.

VI. Conclusion

Implantable biomedical sensors are an attractive solution for health-monitoring and patient-centric healthcare. They hold potential benefits such as improved quality of care, shorter hospitalization times, and reduction of pain and medical complications. Such sensors are best realized in very small form factors, placing stringent limits on system power consumption due to small battery capacity and energy harvesting capability. This paper introduced a mm-scale sensing system platform with a heterogeneous stackable multi-layer structure and described a variety of circuit techniques that can be used for miniaturized biomedical sensors.

References

[1] P. Dario, et al., "Micro-systems in biomedical applications," *J. Micromechan. Microeng.*, vol. 10, no. 2, pp. 235-244, June 2000.

[2] R. A M Receveur, et al., "Microsystem technologies for implantable applications," *J. Micromechan. Microeng.*, vol. 17, no. 5, pp. R50-R80, May 2007.

[3] S. Ayazian, et al., "A Photovoltaic-Driven and Energy-Autonomous CMOS Implantable Sensor," *IEEE TBioCAS*, vol. 6, no. 4, pp. 336-343, Aug. 2012.

[4] D. Jeon, et al., "An Implantable 64nW ECG-Monitoring Mixed-Siganl SoC for Arrhythmia Diagnosis," *IEEE ISSCC*, Feb. 2014, pp. 416-417.

[5] T. Morrison, et al., "A 0.5 cm^3 Four-Channel 1.1 mW Wireless Biosignal Interface With 20 m Range," *IEEE TBioCAS*, vol. 8, no. 1, pp. 138-147, Feb. 2014.

[6] E. Y. Chow, et al., "A Miniature-Implantable RF-Wireless Active Glaucoma Intraocular Pressure Monitor," *IEEE TBioCAS*, vol. 4, no. 6, pp. 340-349, Dec. 2010.

[7] M. H. Ghaed, et al., "Circuits for a Cubic-Millimeter Energy-Autonomous Wireless Intraocular Pressure Monitor," *IEEE TCAS-I,* vol. 60, no. 12, pp. 3152-3162, Dec. 2013.

[8] Y.-C. Shih, et al., "A 2.3µW Wireless Intraocular Pressure/Temperature monitor," *IEEE JSSC*, vol. 46, no. 11, pp. 2592-2601, Nov. 2011.

[9] W. Biederman, et al., "A Fully-Integrated, Miniaturized (0.125 mm^2) 10.5 µW Wireless Neural Sensor," *IEEE JSSC*, vol. 48, no. 4, pp. 960-970, Apr. 2013.

[10] M. Yin, et al., "A 100-Channel hermetically Sealed Implantable Device for Chronic Wireless Neurosensing Applications," *IEEE TBioCAS*, vol. 7, no. 2, pp. 115-128, Apr. 2013.

[11] P.-T. Huang, et al., "2.5D heterogeneously integrated bio-sensing microsystem for multi-channel neural-sensing applications," *IEEE ISSCC*, Feb. 2014, pp. 320-321.

[12] P. Cong, et al., "A Wireless and Batteryless 10-Bit Implantable Blood Pressure Sensing Microsystem With Adaptive RF Powering for Real-Time Laboratory Mice Monitoring," *IEEE JSSC*, vol. 44, no. 12, pp. 3631-3644, Dec. 2009.

[13] K. Watabe, et al., "Hyperthermia Implant Consisting of Resonant Circuit Delivered to Tumor Through 18 G Needle," *IEEE Trans. Magn.*, vol. 47, no. 10, pp. 2887-2889, Oct. 2011.

[14] B. C. Towe, et al., "Wireless Microstimulators for Treatment of Peripheral Vascular Disease," *Int. IEEE EMBS Conf. Neural Engineering*, 2013, pp. 1485-1488.

[15] G. Chen, et al., "Circuit Design Advances for Wireless Sensing Applications," *Proceeding of the IEEE*, vol. 98, no. 11, pp. 1808-1827, Nov. 2010.

[16] http://www.cymbet.com.

[17] Y. Lee, et al., "A Modular 1 mm^3 Die-Stacked Sensing Platform With Low Power I^2C Inter-Die Communication and Multi-Modal Energy Harvesting," *IEEE JSSC*, vol. 48, no. 1, pp. 229-242, Jan. 2013.

[18] R. Haque and K. D. Wise, "Method of embedding material in a glass substrate," U.S. Patent Application 12/581,695, Oct. 19, 2009.

[19] R. Haque, et al., "Implantable device and surgical implantation technique," U.S. Patent Application 13/154,291, Jun. 6, 2011.

[20] D. G. Janagama and R. R. *Tummala, Nanobiosensing Electronics and Nanochemistry for Biosensor Packaging*. New York: Springer, 2010, pp. 613–663.

[21] G. Kim, et al., "A Millimeter-Scale Wireless Imaging System with Continuous Motion Detection and Energy Harvesting," *IEEE VLSIC*, June 2014.

[22] H. Danneels, et al., "A Fully-digital, 0.3V, 270nW Capacitive Sensor Interface Without External References," *IEEE ESSCIRC*, 2011, pp. 287-290.

[23] S. Xia, et al., "A Capacitance-to-Digital Converter for Displacement Sensing with 17b Resolution and 20µs Conversion Time," *IEEE ISSCC*, Feb. 2012, pp. 198-199.

[24] Z. Tan, et al., "A 1.2V 8.3nJ Energy-Efficient CMOS Humidity Sensor for RFID Applications," *IEEE VLSIC*, June 2012, pp. 24-25.

[25] M. A. P. Pertijs and Z. Tan, "Nyquist AD Converters, Sensor Interfaces, and Robustness: Chapter 8. Energy-Efficient Capacitive Sensor Interface," Springer/New York, pp. 129-147, 2013.

[26] H. Ha, et al., "A 160nW 63.9fJ/conversion-step Capacitance-to-Digital Converter for Ultra-Low-Power Wireless Sensor Nodes," *IEEE ISSCC*, Feb. 2014, pp. 220-221.

[27] C. Zellerhoff, et al., "How can we identify the best implantation site for an ECG event recorder?," *Pacing & Clinical Electrophysiol*, vol. 23, no. 10.1, pp. 1545-1549, Oct. 2000.

[28] F. Zhang, et al., "A Batteryless 19µW MICS/ISM-Band Energy Harvesting Body Area Sensor Node SoC," *IEEE ISSCC*, Feb. 2012, pp. 298-299.

[29] S.-Y. Hsu, et al., "A Sub-100µW Multi-Functional Cardiac Signal Processor for Mobile Healthcare Applications," *IEEE VLSIC*, June 2012, pp. 156-157.

[30] S. Kim, et al., "A 20µW Intra-Cardiac Signal-Processing IC with 82dB Bio-Impedance measurement Dynamic Range and Analog Feature Extraction for Ventricular Fibrillation Detection," *IEEE ISSCC*, Feb. 2013, pp. 302-303.

[31] V. Ng and S. Sanders, "A 92%-Efficiency Wide-Input-Voltage-Range Switched-Capacitor DC-DC Converter," *IEEE ISSCC*, Feb. 2012, pp. 282-283.

[32] Y. K. Ramadass, et al., "A Fully-Integrated Switched-Capacitor Step-Down DC-DC Converter With Digital Capacitance Modulation in 45nm CMOS," *IEEE JSSC*, vol. 45, no. 12, pp. 2557-2565, Dec. 2010.

[33] Y. K. Ramadass and A.P. Chandrakasan, "Voltage Scalable Switched Capacitor DC-DC Converter for Ultra-Low-Power On-Chip Applications," *IEEE PESC*, pp. 2353-2359, June 2007.

[34] S. Bang, et al., "A Fully Integrated Successive-Approximation Switched-Capacitor DC-DC Converter with 31mV Output Voltage Resolution," *IEEE ISSCC*, Feb. 2013, pp. 370-371.

[35] D. Somasekhar, et al., "Multi-Phase 1 GHz Voltage Doubler Charge Pump in 32 nm Logic Process," *IEEE JSSC*, vol. 45, no. 4. pp. 751-758, Apr. 2010.

[36] T. V. Breussegem and M. Steyaert, "A 82% Efficiency 0.5% Ripple 16-Phase Fully Integrated Capacitive Voltage Doubler," *IEEE VLSIC*, June 2009, pp. 198-199.

[37] I. Doms, et al., "Integrated Capacitive Power management Circuit for Thermal Harvesters with Output Power 10 to 1000µW," *IEEE ISSCC*, Feb. 2009, pp. 300-301.

[38] W. Jung, et al., "A 3nW Fully Integrated Energy Harvester Based on Self-Oscillating Switched-Capacitor DC-DC Converter," *IEEE ISSCC*, Feb. 2014, pp. 398-399.

[39] H. J. Bergveld, et al., "Battery management Systems: Design by Modelling," Springer, 2002.

[40] Texas Instruments, "Impedance Track™ Gas Gauge for Novices," Jan. 2006.

[41] I. Lee, et al., "Low Power Battery Supervisory Circuit with Adaptive Battery Health monitor," *IEEE VLSIC*, June 2014.

[42] S. Drago, et al., "A 2.4 GHz 830pJ.bit duty-cycled wake-up receiver with -82dBm sensitivity for crystal-less wireless sensor nodes," *IEEE ISSCC*, Feb. 2010, pp. 224-225.

[43] N. Pletcher, et al., "A 52µW Wake-Up Receiver With -72 dBm Sensitivity Using an Uncertain-IF architecture," *IEEE JSSC*, vol. 44, no. 1, pp. 269-280, Jan. 2009.

[44] K. Yadav, et al., "A 4.4µW Wake-Up Receiver using Ultrasound Data Communications," *IEEE VLSIC*, June 2011.

[45] G. Kim, et al., "A 695 pW Standby Power Optical Wake-up Receiver for Wireless Sensor Nodes," *IEEE CICC*, Sep. 2013, pp. 1-4.

[46] S. Mandal and R. Sarpenshka, "Power-efficient impedance-modulation wireless data links for biomedical implants," IEEE *TBioCAS*, vol. 2, no. 4, pp. 301-315, Dec. 2008.

[47] G. Wang, et al., "Design and analysis of an adaptive transcutaneous power telemetry for biomedical implants," *IEEE TCAS-I*, vol. 52, no. 10, pp. 2109-2117, Oct. 2005.

[48] Y.-S. Lin, et al., "Near-field communication using phase-locking and pulse signaling for millimeter-scale systems," *IEEE CICC*, Sep. 2009, pp. 563-566.

[49] X. Huang, et al., "A 915 MHz 120µW-RX/900µW-TX envelope detection transceiver with 20 dB in-band interference tolerance," *IEEE ISSCC*, Feb. 2012, pp. 454-456.

[50] J. Choi, et al., "An interference-aware 5.8 GHz wake-up radio for ETCS," *IEEE ISSCC*, Feb. 2012, pp. 446-448.

[51] NXP Semiconductors, "I^2C-bus specification and user manual, UM10204 datasheet, Rev. 3," June 2007.